Transdermal delivery of allopurinol on acute hyperuricemic mice via polymer microneedles for regulation of serum uric acid levels

Rui Wang, Han Wang, Guohua Jiang*, Yanfang Sun, Tianqi Liu, Khaydar E. Yunusov, Uladzislau E. Aharodnikau, Lei Nie, Amin Shavandi

Rui Wang, Guohua Jiang, Tianqi Liu
School of Materials Science and Engineering, Zhejiang Sci-Tech University, Hangzhou, China
International Scientific and Technological Cooperation Base of Intelligent Biomaterials and Functional Fibers, Zhejiang Sci-Tech University, Hangzhou, China
E-mail: ghjiang_cn@zstu.edu.cn (G. Jiang)

Han Wang
Wenzhou Institute, University of Chinese Academy of Sciences, Wenzhou, China

Yanfang Sun
College of Life Sciences and Medicine, Zhejiang Sci-Tech University, Hangzhou, Zhejiang, China

Khaydar E. Yunusov
Institute of Polymer Chemistry and Physics, Uzbekistan Academy of Sciences, Tashkent, Uzbekistan

Uladzislau E. Aharodnikau
Research Institute for Physical Chemical Problems, Belarusian State University, Minsk, Belarus

Lei Nie
College of Life Science, Xinyang Normal University, Xinyang, China

Amin Shavandi
3BIO-BioMatter, École polytechnique de Bruxelles, Université Libre de Bruxelles (ULB), Brussels, Belgium

Abstract: Allopurinol (AP) is widely used to treat hyperuricemia which may cause severe side effects after oral administration. Alternative means for the treatment of hyperuricemia are demanded to simultaneously facilitate drug absorption, patient compliance, and fewer side effects. In this study, a new polymer microneedles (MNs) system was developed for transdermal delivery of AP on acute hyperuricemic mice. This study aims to achieve the controllable regulation of serum uric acid (SUA) levels with fewer side effects compared with oral administration. The matrix of polymer MNs consisted of polyvinylpyrrolidone (PVP) and polycaprolactone (PCL), in which the rapid dissolution of PVP offers a rapid dissolution of AP into the blood and the biodegradability of PCL resulting in a sustainable drug release behavior. An *in vivo* study demonstrated that the AP-loaded MNs system can effectively reduce the SUA levels as oral administration with lower side effects, which will conducive to reducing the adverse reactions and improving the bioavailability of AP. This MNs-mediated strategy can facilitate transcutaneous hyperuricemia treatment and provide a new alternative for the exploration of clinical treatment of hyperuricemia and improvement of patient compliance.

1. Introduction

Gout, a common chronic disease caused by the deposition of monosodium urate (MSU) crystal in articular and non-articular structures, has a substantial disease burden and is increasing in different ethnic groups and regions, which may become a modern gout epidemic analogous to the obesity epidemic [1-6]. The progression of gout can be divided into multiple stages [7,8]. The first is the development of hyperuricaemia, which is an essential but not sufficient step for the development of gout [2,9]. The majority of people with hyperuricaemia will not suffer from gout, even after prolonged periods of observation [7]. In addition, it estimates that hyperuricaemia prevalence in China is 13.3%, while that of gout is 1.1%. Hence, hyperuricemia may not necessarily develop into gout, but the probability of gout will be greatly increased with sustained hyperuricemia, which is a physiological prerequisite for gout [1,2,10]. Inspired by this, we tried to prevent people from suffering from gout by treating hyperuricemia in advance.

Non-drug therapy, such as diet, reduce the intake of purine-rich foods (beer, meat, and seafood) and increase water consumption, provide physical barriers for hyperuricemia patient, but these barrier approaches generally have high failure rates due to poor patient compliance and acceptance [11-13]. Controlling uric acid (UA) production is the best way to prevent and treat hyperuricemia through drug therapy [2]. In the past decades, AP has been used as the most anti-hyperuricemia drug [14] to control hyperuricemia and gout and to reduce the complications of cardiovascular disease and renal failure [15]. However, using drugs for the treatment of hyperuricemia may give rise to serious side effects such as gastrointestinal intolerance, liver/kidney damage, allergy, and central nervous system disorders [16-18]. Therefore, it is urgent to find a way to accelerate drug absorption, avoid the first-pass effect and increase drug efficacy, which will improve the bioavailability of anti-hyperuricemia drugs [19-23].

Microneedles (MNs) are micrometre-scale structures that penetrate the stratum corneum of the skin to deliver drugs in a minimally invasive manner and can be utilized as a new drug delivery system [24-32]. Given the potential of MNs for minimally invasive and self-administration without professional training, the application of MNs has grown rapidly.

Hitherto, MNs have been used for the delivery of drugs, which include insulin [33,34], vaccines [35-37], protein, and various high molecular weight compounds [30,38]. Several diagnostic applications of MNs have been reported which are largely based on using MNs for drawing blood or other fluids for biomarkers detection [39,40].

Given that MNs can effectively penetrate the epidermis and deliver drugs, MNs also have been reported for skin wound healing [41,42].

Among the several different types of MNs, the matrix of dissolvable MNs is comprised of biocompatible and biodegradable polymers, such as polyvinylpyrrolidone (PVP) [43-45], a water-soluble polymer widely used in the pharmaceutical industry, and polycaprolactone (PCL), a biodegradable and biocompatible polymer with a low melting temperature of 59-64 °C [46,47], which is approved by US FDA for use in a variety of medical devices [48-51].

In this study, we presented a new MNs system for transdermal delivery of AP on acute hyperuricemic mice. This study aims to achieve the controllable regulation of serum uric acid (SUA) levels with fewer side effects when administered by MNs. The matrix of MNs consisted of PVP and PCL, in which the rapid dissolution of PVP offers a rapid dissolution of AP into the blood, and the biodegradability of PCL resulting a sustainable drug release behavior. The chemical, morphological and mechanical properties of the MNs were investigated, and then *in vivo* studies were performed to compare the efficacy and side effects of oral and MNs treatment on SUA levels. We envisage that this AP-loaded MNs system can provide a new avenue to increase acute-hyperuricemic patients' compliance and reduce side effects.

2. Materials and method

2.1 Materials

Polyvinylpyrrolidone (PVP M_W = 58 KDa), polycaprolactone (PCL M_W = 45 KDa), polyvinyl alcohol (PVA, 1788 type, alcoholysis= 87.0-89.0%), potassium oxonate (98%, M_W =195.18) and hypoxanthine (99%) were purchased from Macklin Biochemical Co., Ltd. (Shanghai, China). Allopurinol (AP, 98%) and rhodamine 6G (R6G) were obtained from Aladdin Chemistry Co. Ltd. (Shanghai, China). Serum uric acid (UA)(Art. No. E-BC-K016-M), serum creatinine (SCr) (Art. No. E-BC-K188-M), nitric oxide (NO) colorimetric assay kit(Art. No. E-BC-K035-M) and adenosine deaminase (ADA) activity assay kit (Art. No. E-BC-K197-M) were obtained from Elabscience Biotechnology Co., Ltd. (Wuhan, China). Strat-M membranes with a diameter of 25 mm and thickness of 300 μm were purchased from Shanghai Xuanyi Environmental Protection Technology Co., Ltd. (Shanghai, China).

2.2 Design and fabrication of MNs

The fabrication process of the AP-loaded MNs is shown in **Figure 1a**. PCL and PVP with a weight ratio of 1:3 were dissolved in solvent (dichloromethane/ethanol, 50/50 in v/v). Under magnetic stirring at 400 rpm for 60 min, a homogeneous solution with a concentration of ~40 wt. % was formed. Then, AP was dissolved in the polymer solution to achieve a concentration of ~ 43 wt. %. The as-obtained solution was filled into the PDMS mold (20 × 20 arrays) by

vacuum pumping, and the excess solution on the surface was scraped off. Thereafter, an aqueous solution of PVA/PVP (20 wt%) was pipetted onto the mold to form the patch backing layer. After completely drying for 12 h at 45 °C, the dried MNs were carefully peeled off and finally sealed and placed in a vacuum incubator for further analysis. The structure, morphology, and geometric dimensions of the fabricated MNs were visualized by scanning electron microscopy (SEM, Vltra55, Zeiss, Germany) and three-dimensional laser scanning confocal microscope (LSCM, C2, Nikon Corporation, Japan).

2.3 Mechanical strength measurement

To explore whether the MNs have sufficient strength to pierce the skin, the mechanical properties of MNs were evaluated by compression tests. Before and after the compression test, the morphological changes of MN_S were observed by an optical microscope (OM, Imager A1m). In addition, the skin embedding and insertion potentials were examined by an *ex vivo* skin insertion test.

2.4 *In vitro* drug release study

The prepared MNs were put into vials containing 20 mL of PBS, and the vials were incubated in a water bath at 37 °C. Thereafter, at distinct time intervals, a 3 mL aliquot was taken out from each sample and supplemented with an equal volume of PBS. Eventually, the amounts of AP released from the MNs were quantitatively analyzed by ultraviolet-visible spectrophotometer (UV, TU-1901, Beijing Purkinje General Instrument Co., Ltd., China).

To further investigate drug diffusion and absorption through the skin, a Franz diffusion cell system was developed for *in vitro* transdermal absorption detection (**Figure S1**). Briefly, 25 mL of PBS was added to the receiving chamber (the level of PBS buffer was exactly 1 mm higher than the surface of the skin *in vitro* to ensure stable contact between the PBS and the mouse skin during the sampling process). Then, the Strat-M membrane inserted with the MN patch was used as a carrier and fixed between the receiving chamber and supply chamber of the Franz diffusion cell. The as-assembled Franz diffusion cell was incubated in a water bath at 37 °C with magnetic stirring of 350 r/min. At distinct intervals, a 3 mL aliquot was taken out from the sampling port and replenished with an equal amount of PBS. Ultimately, the amount of the drug was determined by UV spectrophotometry.

2.5 *In vivo* pharmacodynamic study

ICR mice (male, 20-22 g, Wenzhou Research Institute, Chinese Academy of Sciences) were used in this study. Animal studies were conducted in line with the regulations on the care and use of laboratory animals. All animal procedures were sanctioned by the Animal Ethics Committee of Zhejiang Sci-Tech University (acceptance number: 2019-02-01) and performed

in Wenzhou Research Institute, Chinese Academy of Sciences. Two different induction protocols were firstly tested: (1) intraperitoneal injection of hypoxanthine (500 mg/kg) combined with subcutaneous injection of potassium oxonate (100 mg/kg) to obtain a hyperuricemia mice model (2) intraperitoneal injection of hypoxanthine (500 mg/kg) combined with subcutaneous injection of potassium oxonate (400 mg/kg) to get another model of hyperuricemic mice. Three mice per group were used to do the statistical study.

At distinct intervals, the mice were bled from the orbit and placed in a refrigerator at 4 °C overnight. The serum was obtained by centrifuging the collected blood at 3000 r/min for 10 min and placing it in a refrigerator at 4°C to determine the amount of serum uric acid (SUA), serum creatinine (SCr), and nitric oxide (NO) by colorimetry. The specific operation process is to use the microplate reader to detect the absorbance of the standard hole and the measuring hole under specified conditions at the optimal detection wavelength, and then use the formula on the biochemical assay kit to obtain the results.

2.6 Histological and immunohistochemical analysis

The mice were sacrificed and their organs (heart, liver, spleen, lung, and kidney) were retrieved. Subsequently, part of the liver tissue was taken and instantly snap-frozen in liquid nitrogen, and then stored at -80 °C to measure the activity of ADA in the liver. Briefly, after weighing the liver tissue block, 9 times the volume of pre-cooled 0.9% sodium chloride solution was added to prepare a 10% tissue homogenate. Afterward, the supernatant was obtained by centrifuging tissue homogenate at 2,500 r/min for 10 min, which was used to measure the ADA activity of the tissue homogenate using colorimetry.

The retrieved kidney tissues were fixed with paraformaldehyde (4%) overnight for histological studies. First, the formol-fixed kidney tissue was dehydrated in graded alcohol (75%, 85%, 95%, and 100%), then cleared in xylene, and finally embedded in paraffin. Then, small sections (~ 5 μm in thickness) were stained with standard hematoxylin-eosin (H&E) solution and examined classically with an optical microscope to identify histopathological lesions.

2.7 Statistical analysis

Statistical analysis of the experimental data was conducted using GraphPad Prism 8.0 (GraphPad Software, Inc., San Diego, CA), and a statistical comparison of analytical values was obtained by one-way ANOVA analysis. A value of $p < 0.05$ (*), 0.01(**), 0.001(***) and 0.0001(****) was considered statistically significant differences. The values were presented as means with standard deviation (S.D.).

3. Results and discussion

3.1 Fabrication of MN patches

To achieve a sustained anti-hyperuricemia effect, a new MNs system is developed for transdermal delivery of AP for regulation of SUA levels in acute hyperuricemic mice. The matrix of MNs consists of PVP and PCL, in which the rapid dissolution of PVP offers rapid delivery of AP into blood [45, 52-53], and the biodegradability of PCL resulting a sustainable drug release and offers a suitable mechanical strength for MNs. Firstly, the mixture of PCL, PVP, and AP is coasted on the PDMS MNs mold to form the needle tips. And the solution of PVA/PVP is poured onto the mold to form the dissolving back patching (**Figure 1b**).
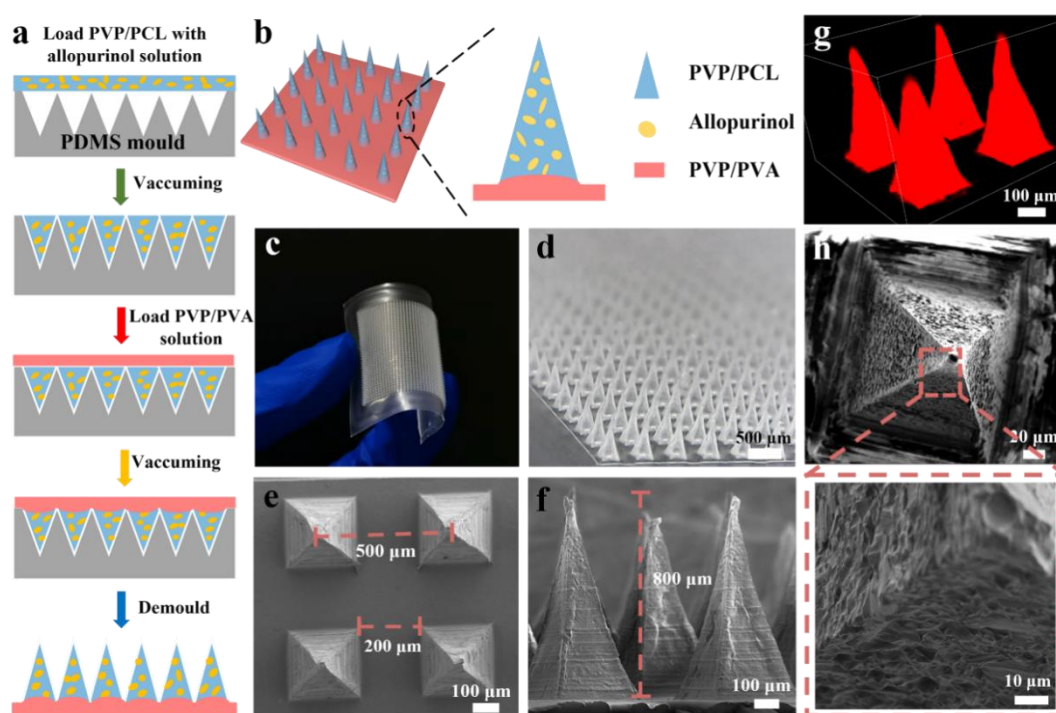

Figure 1. Schematic of the fabrication process of MNs (a), schematic structure of MNs (b), digital images of the as-fabricated MNs (c and d), SEM images of PVP/PCL MNs (e and f), the confocal image of MN arrays (g), and the porous structure of MNs formed by the rapid dissolution of PVP (h).

Figure 1c and **d** display the digital microscope images of the prepared microneedle patch, indicating a flexible back patch and regular microneedle array. The SEM images (**Figure 1e**, **1f**) of the as-fabricated MNs exhibit a pyramidal shape, which is also confirmed by stereomicroscope images (**Figure S2**). The base width of the pyramidal MNs and the spacing between the adjacent needle tips of MNs are ~200 and ~500 μm, respectively. And the height of the MNs is ~800 μm. To further investigate the geometry structure of the MNs, the R6G has been mixed with the homogeneous solution of needle tips when filled into the cavities of the

mold, so that the MNs arrays with red needle tips can be observed using LSCM (**Figure 1g**). In addition, the porous structure of MNs also can be observed after immersion of MNs patches into PBS solution for 5 min due to the high solubility of PVP (**Figure 1h, S3a**), which is beneficial for the rapid release of AP and accelerating the biodegradation of PCL in the body fluid.

3.2 Mechanical properties and drug release of MNs

The mechanical properties of the as-fabricated MNs are tested by compression test. **Figure 2a** shows the force-displacement graph of PVP/PCL and PVP MNs. The pure PVP MNs could tolerate the compressive forces of 0.12 N/needle at 600 µm displacement. However, PVP/PCL MNs could withstand the maximum compressive force of ~ 0.23 N/needle. Although the mechanical strength of pure PVP MNs is sufficient to penetrate the skin [54,55], it can be further improved by mixing PCL into the matrix of needle tips. Moreover, the insets in **Figure 2a** and **Figure S3b** show the morphology of PVP/PCL MNs after the compression test, and no signs of cracking are found, which indicates the excellent toughness of the PVP/PCL MNs. The excellent mechanical strength of PVP/PCL MNs is further confirmed by penetrating MNs into porcine skin. As shown in **Figure 2b**, the porcine skin surface displays an array of needle spots that are corresponded to the puncture sites after the insertion and removal of MNs. **Figure 2c** shows the tissue morphology after insertion by MNs containing R6G. After the MNs penetrate the skin, many microchannels with a depth of ~300-500 µm can be observed, which verifies that the prepared MNs can efficiently penetrate the skin tissue. In addition, red fluorescence signals were found around the puncture sites (**Figure 2d**), which verified that the drugs can be released to the skin tissue due to the dissolution of MNs polymer matrix.
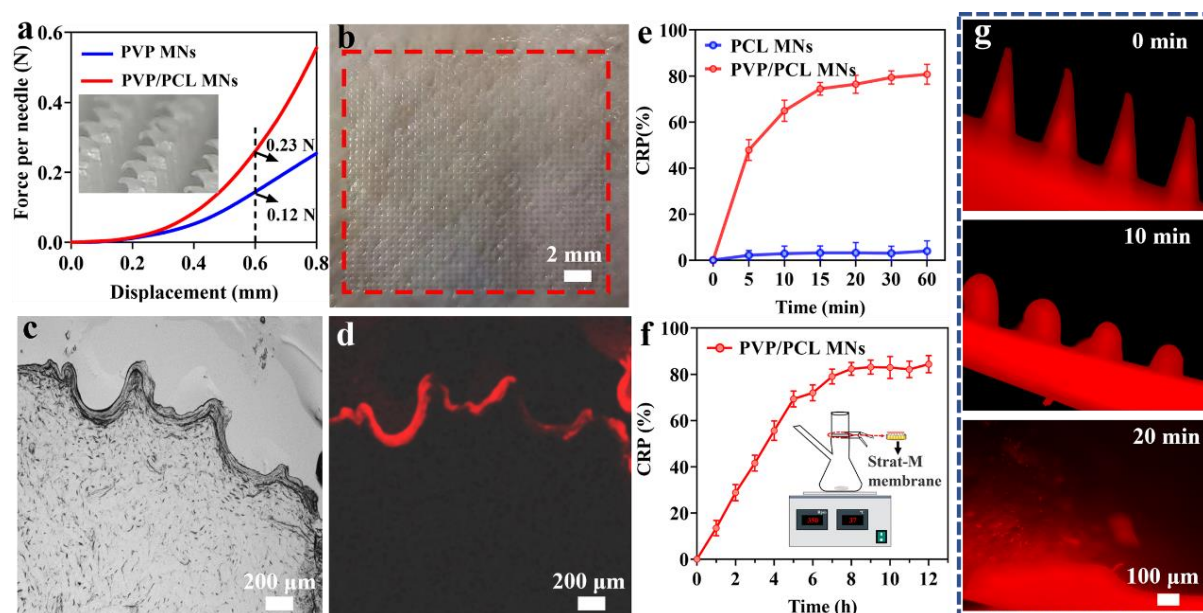
Figure 2. Force-displacement graph of PVP/PCL and PVP MNs (a), digital image of porcine skin after insertion and removal of MNs (b), representative histological images of porcine skin after removal of MNs *ex vivo* (c and d), digital images of MNs dissolution in mouse cadaver skin *ex vivo* for 1, 10, and 20 min (e), *in vitro* AP release curves of MNs in PBS solution (f), and *in vitro* skin drug release profile of AP-loaded PVP/PCL MNs.

To evaluate the drug release behaviors, the cumulated release percentage (CRP) of AP from AP-loaded MNs is tested *in vitro* using PBS solution (pH = 7.4) as the release media. The AP can be rapidly released from MNs within 15 min, as shown in **Figure 2e**. However, almost no drug release was observed from the PCL MNs. To more accurately reflect the penetration and diffusion of the drugs in the skin, Franz diffusion cell was used to conduct an *in vitro* skin drug release test. The schematic of Franz diffusion cell is presented in the inset of **Figure 2f**. The AP-loaded PVP/PCL MNs are applied to Strat-M membrane, which is fixed in the Franz diffusion cell by pressing a pinch clamp. Samples were taken from the sampling port and the amount of AP in each sample is quantitated at different intervals. The AP release profiles of the MNs show a steady increase within the first 7 h, and ~70% of AP can be released after 7 h post-application. It indicates the drug in the MNs can be effectively delivered through the micropores formed by the microneedles penetrating the skin. In addition, the PVP/PCL MN arrays containing R6G were inserted into mouse cadaver skin (**Figure S3c**), and its dissolution over time was monitored. **Figure 2g** shows the fluorescence morphological changes of MNs after insertion of PVP/PCL MNs into the skin for 0, 10, and 20 min. The clear sharp MN edges can be observed before insertion, and they become round after insertion for 10 min and disappeared after 20 min.

3.3 Regulation of SUA *in vivo*

To investigate the regulation of SUA *in vivo*, the hyperuricemia model on ICR mice is established by intraperitoneal injection of hypoxanthine and subcutaneous injection of potassium oxonate. The SUA level can be reached the maximum level at ~520 μmol/L, 3 times higher than the normal state, after intraperitoneal injection of hypoxanthine (~500 mg/kg) and subcutaneous injection of potassium oxonate (100 mg/kg) for 2 h. And then, the SUA level will be decreased slowly to ~250 μmol/L after injection for 6 h due to the presence of the urate oxidase (UOX) gene in mice, which can oxidize SUA into allantoin, and allantoin is more soluble in water than SUA and easier to be excreted with urine [56] (**Figure S4**). However, the high SUA level can be maintained at the higher levels for intraperitoneal injection of hypoxanthine (~500 mg/kg) and subcutaneous injection of potassium oxonate (400 mg/kg). The

maximum level (~650 μmol/L) can be obtained after the injection for 1.5 h, and it still can be maintained at ~500 μmol/L after 6 h (**Figure S5**). Therefore, the latter method has been adopted for establishing the hyperuricemia model.

The therapeutic efficiency of the delivery of AP via MNs was evaluated *in vivo* on the hyperuricemia model. The hyperuricemia mice are randomly divided into 4 groups after modeling: (I) control group (health), (II) model group (without any treatment), (III) oral group (treatment by oral AP), (IV) MN group (treatment by AP-loaded PCL or PVP/PCL MNs), as shown in **Figure 3a**. Note that, when AP-loaded MNs were manually applied to mice skin *in vivo* and gently pressed, the MNs penetrated the skin and embedded completely under the skin surface (**Figure S6a**). **Figure 3b** shows the profile of SUA levels against time in the different groups after treatment. The SUA level can be kept at a stability state at ~150 μmol/L in the health group. In the case of the model group, the SUA level can be decreased slowly from ~650 μmol/L to ~500 μmol/L after 5 h. After oral treatment by AP (20 mg/kg) the SUA level can be decreased slowly from ~600 μmol/L after 1 h to ~300 μmol/L after 5 h. However, the SUA level has a slight decrease (from ~650 to 480 μmol/L) for the AP-loaded PCL MNs, although the same dose amount with the oral group. It can be contributed to the slow degradation of PCL in the body. The hyperuricemia model treated by AP-loaded /PVP/PCL MNs exhibits the best treatment in all groups. After treatment for 1 h, the SUA level is ~550 μmol/L. And it further decreased to the lowest concentration at ~157.49 ± 23.46 μmol/L after 3h which is close to the level in the health group. After that, the SUA levels still can be maintained at the therapeutic level (~150 μmol/L) for 5 h, showing a longer time for inhibiting the increase of SUA levels and the best treatment effect in all groups. It mainly contributed to the composition of the matrix of MNs. Some drugs are released rapidly following the dissolution of PVP, resulting in rapid diffusion of AP into blood similar to the oral delivery route. And the biodegradability of PCL also can be accelerated due to the dissolution of PVP. The AP loaded in PCL can be served as a drug reservoir for sustained drug release.
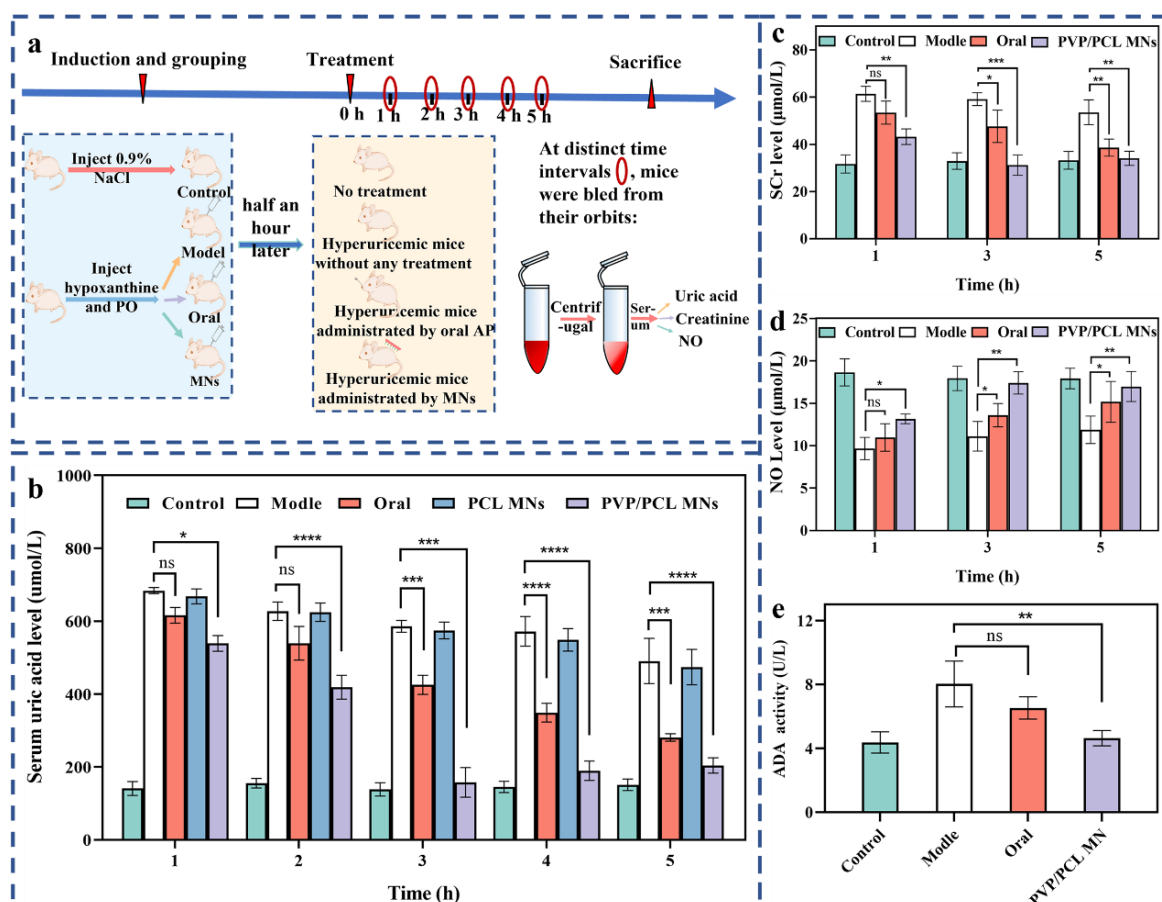
Figure 3. The animal experiment process via polymer MNs for regulation of SUA levels (a), the SUA (b), SCr (c) and NO (d) levels of the mice treated by AP-loaded PVP/PCL MNs compared with the healthy model, oral and PCL MNs groups, and ADA activity from liver tissue of the mice treated by AP-loaded PVP/PCL MNs compared with healthy, model and oral groups (e).

3.4 Blood and immunohistochemical analysis

SCr is the most commonly used screening test for kidney and renal function, and its high concentration is associated with renal function injury [57,58]. So, the SCr levels can be used to determine renal function. **Figure 3c** shows the SCr levels for all groups. The SCr in the model group shows the highest levels in all groups at different intervals, indicating the most severe kidney and renal damage due to no drug treatment. In the case of the oral group, the SCr levels show a slow decrease trend from 1 to 5 h treatment. Although the SCr levels exhibit a similar trend in the PVP/PCL MNs group, they are lower than that in the oral groups at all intervals. Importantly, the SCr levels (~32 μmol/L) are close to the health group after 5 h treatment. It indicates that negligible kidney and renal function damage is induced by the MN treatment because of the lower AP concentration in the blood compared with that in the oral group.

In addition, NO (also known as an endothelial-derived relaxing factor, EDRF), as an important mediator regulating vascular tone, is also affected by the decrease of renal blood flow that caused the impairment of vasodilation function [58,59]. Therefore, the level of NO is another biomarker for hyperuricemia [60]. **Figure 3d** shows the NO levels in all groups at different intervals. At 1h, no significant difference was found in all experimental groups. However, higher NO levels in PVP/PCL MNs groups are enrolled in this study compared to the model and oral groups, which is reach the normal level after 5 h treatment.

Adenosine deaminase (ADA) is an important enzyme in nucleoside metabolism [61]. The increase in ADA activity will promote the catabolism of nucleic acid and lead to an increase in SUA production [61]. Therefore, inhibition of ADA activity can efficiently reduce the concentration of UA [62]. To determine the hepatic activity of ADA, the ADA activities from liver tissue are tested using commercial ADA activity assay kit. As shown in **Figure 3e**, after 5 h, compared with the control group, the ADA activity of the model group increased significantly. However, significant inhibiting hepatic ADA activity occurred in oral and PVP/PCL MNs groups compared with the model group. Especially in the PVP/PCL MNs group, it remains at a relatively low level close to the healthy group and is significantly lower than that of the model group. Taken together, MNs treatment can effectively promote the secretion of SCr and NO, and inhibit the activity of ADA in mice, thereby reducing the production of SUA. The relative higher ADA activity in the oral group may be contributed to the liver damage caused by oral administration.

3.5 Histopathology analysis

The treated mice were sacrificed and the heart, liver, spleen, lung, and kidney tissues were retrieved (**Figure 4a**). No tissue lesions occurred in the heart, spleen, and lung (**Figure S6b**). No significant drastic liver and kidney changes are found in the PVP/PCL MNs groups compared with the control group, suggesting that the MNs administration did not cause remarkable liver damage and renal impairment. On the contrary, acute liver and kidney damage has been found in the model group, which has been confirmed by the increase of SCr and ADA levels. In addition, traditional oral drug administration also shows severe liver toxicity due to the first-pass effect and slow clearance. Hence, the MN-mediated strategy explored in this study can be used as an attractive anti-hyperuricemia treatment with lower damage, toxicity, and longer therapeutic effect.
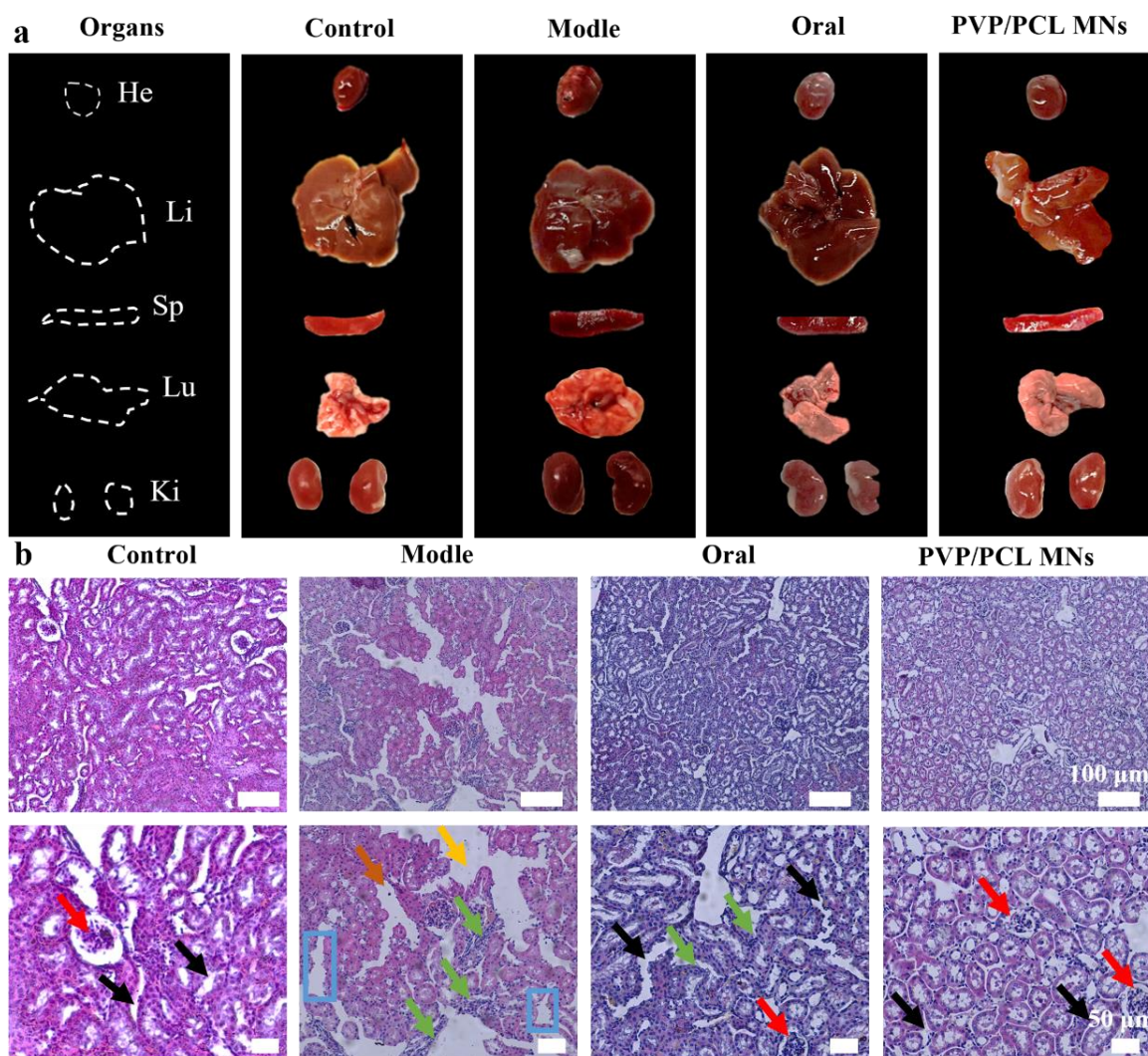
Figure 4. The images of major organs (heart, liver, spleen, lung, and kidney) retrieved from the mice (a) and H&E staining images of kidney tissue slices from treated mice (b) (red arrow: normal glomerulus morphology, black arrow: complete brush border structure, yellow arrow: dilatation of renal tubule, orange arrow: renal tubular epithelial cell necrosis, green arrow: renal interstitial inflammatory cell infiltration, blue square frame: the disappearance of brush border).

The kidney is an important functional organ for urine production. However, high SUA levels can cause damage to the glomerulus, renal tubule, and epithelial cells of the renal tubular [63]. For this reason, histological studies of renal parenchyma were performed. As shown in **Figure 4b**, the kidney section of blank control shows the regular cell arrangement, normal hepatic architecture, and glomerulus morphology without inflammation or necrosis. However, the hyperuricemic model group depicts mild tubular edema. In addition, the dilatation of renal tubules, degeneration of tubule epithelial cells, and disappearance of the brush border of epithelial cells were also observed in the model group. In the oral group, some whites were

observed on the surface of renal tissue, revealing some severe nephrotoxicity. Meanwhile, the phenomenon of inflammatory cell infiltration in renal interstitium was also found, which indicates that oral administration deepens kidney damage. However, the kidney section of the PVP/PCL MNs group shows normal glomerulus morphologies and complete brush border structure, which was similar to the control group, suggesting that it could validly alleviate the renal histopathological damages in hyperuricemic mice. In short, MNs-mediated strategies not only have a significant hypouricmic effect but also have protective effects on liver and kidney tissues.

4. Conclusion

In view of the limited clinical efficacy and severe side effects of conventional oral AP in the treatment of hyperuricemia and gout. Herein, we proposed AP encapsulated in PVP/PCL composite MNs by the mold casting method to regulate SUA levels, realize the sustained drug release and reduce or even reverse the damage to the kidney. The mechanical strength of as-fabricated MNs have sufficient potential to pierce the skin and release the AP in a sustained pattern due to the dissolution and degradation differences of raw materials in MNs matrix. An *in vivo* study demonstrated that the AP-loaded MNs system can effectively reduce the SUA levels as oral administration with lower side effects, which will contribute to reducing liver and kidney damage and improve the bioavailability of AP. Thus, this MNs-mediated strategy can facilitate transcutaneous hyperuricemia treatment and provide a new alternative for the exploration of clinical treatment of hyperuricemia.

Supporting Information

Supporting Information is available from the Wiley Online Library or from the author.

Acknowledgments

Conflict of interests

The authors declare that they have no conflicts of interest to this work.

Author contributions

Data Availability Statement

The data that support the findings of this study are available from the corresponding author upon reasonable request.

References

[1] N. Dalbeth, A. L. Gosling, A. Gaffo, A. Abhishek, *Lancet.* **2021**, *397*, 1843.

[2] N. Dalbeth, H. K. Choi, L. A. B. Joosten, P. P. Khanna, H. Matsuo, F. Perez-Ruiz, L. K. Stamp, *Nat. Rev. Dis. Primers.* **2019**, *5*, 69.

[3] J. A. Singh, I. Herbey, A. Bharat, J. E. Dinnella, S. Pullman-Mooar, S. Eisen, N. Ivankova, *Arthritis Care Res.* **2017**, *69*, 1724.

[4] M. Toprover, S. Krasnokutsky, M. H. Pillinger, *Curr. Rheumatol. Rep.* **2015**, *17*, 70.

[5] M. Chen-Xu, C. Yokose, S. K. Rai, M. H. Pillinger, H. K. Choi, *Arthritis Rheumatol.* **2019,** *71*, 991.

[6] C. -F. Kuo, M. J. Grainge, W. Y. Zhang, M. Doherty, *Nat. Rev. Rheumatol.* **2015**, *11*, 649.

[7] N. Dalbeth, P. -G. Amanda, C. Frampton, T. Neogi, W. J. Taylor, T. R. Merriman, *Ann. Rheum. Dis.* **2018**, *77*, 1048.

[8] N. Dalbeth, L. Stamp, *Ann. Rheum. Dis.* **2014**, *73*, 1598.

[9] N. Dalbeth, M. E. House, O. Aati, P. Tan, C. Franklin, A. Horne, G. D. Gamble, L. K Stamp, A. J. Doyle, F. M. McQueen, *Ann. Rheum. Dis.* **2015**, *74*, 908.

[10] A. Shiozawa, S. M. Szabo, A. Bolzani, A. Cheung, H. K. Choi, *J. Rheumatol.* **2017**, *44*, 388.

[11] H. K. Choi, S. Liu, G. Curhan, *Arthritis Rheum.* **2005**, *52*, 283.

[12] H. K. Choi, K. Atkinson, E. W. Karlson, W. Willett, G. Curhan, *Lancet.* **2004**, *363*, 0.

[13] H. Nan, Q. Qiao, Y. H. Dong, W. G. Gao, B. Tang, R. L. Qian, J. Tuomilehto, *J. Rheumatol.* **2006**, *33*, 1346.

[14] N. Dalbeth, K. Billington, A. Doyle, C. Frampton, P. Tan, O. Aati, J. Allan, J. Drake, A. Horne, L. K. Stamp, *Arthritis Rheumatol.* **2019**, *71*,1739-1746.

[15] F. Mozaffari, S. M. H. Razavian, M. A. Ghasemzadeh, *J. Pharm. Innov.* **2022**. 10.1007/s12247-022-09624-2.

[16] F. K. Aldawood, A. Andar, S. Desai, *Polymers.* **2021**, *13*, 2815.

[17] M. A. Sawon, M. F. Samad, *J. Drug Deliv. Sci. Tec.* **2021**, *63*, 102477.

[18] S. Mdanda, P. Ubanako, P. P. D. Kondiah, P. Kumar, Y. E. Choonara, *Polymers.* **2021**, *13*, 2405.

[19] B. Xu, Q. Y. Cao, Y. Zhang, W. J. Yu, J. Y. Zhu, D. P. Liu, G. H. Jiang, *ACS Biomater. Sci. Eng.* **2018**, *4*, 2473.

[20] G. Song, G. H. Jiang, T. Q. Liu, X. Y. Zhang, Z. Y. Zeng, R. F. Wang, P. F. Li, Y. H. Yang, *ACS Biomater. Sci. Eng.* **2020**, *6*, 4116.

[21] B. Homayun, X. T. Lin, H. -J. Choi, *Pharmaceutics.* **2019**, *11*, 129.

[22] L. M. Ruan, G. Song, X. Y. Zhang, T. Q. Liu, Y. F. Sun, J. L. Zhu, Z. Y. Zeng, G. H. Jiang, *Biomater. Sci.* **2021**, *9*, 6830.

[23] H. Juster, B. van der Aar, H. de Brouwer, *Polym. Eng. Sci.* **2021**, *59*, 877.

[24] X. X. Zhang, G. P. Chen, L. Y. Sun, F. F. Ye, X. Shen, Y. J. Zhao, *Chem. Eng. J.* **2021**, *406*, 126741.

[25] Y. Zhang, G. H. Jiang, W. J. Yu, D. P. Liu, B. Xu, *Mat. Sci. Eng. C.* **2018**, *85*, 18.

[26] Z. J. Fan, Y. Wei, Z. R. Yin, H. F. Huang, X. Z. Liao, L. Y. Sun, B. Liu, F. Z. Liu, *ACS Appl. Mater. Inter.* **2021**, *13*, 40278.

[27] R. K. Mishra, K. Y. Goud, Z. H. Li, C. Moonla, M. A. Mohamed, F. Tehrani, H. Teymourian, J. Wang, *J. Am. Chem. Soc.* **2020**, *142*, 5991.

[28] R. Jamaledin, C. Di Natale, V. Onesto, Z. B. Taraghdari, E. N. Zare, P. Makvandi, R. Vecchione, P. A. Netti, *J. Clin. Med.* **2020**, *9*, 542.

[29] R. Jamaledin, C. K. Y. Yiu, E. N. Zare, L.-N. Niu, R. Vecchione, G. J. Chen, Z. Gu, F. R. Tay, P. Makvandi, *Adv. Mater.* **2020**, *32*, 2002129.

[30] R. Wang, G. H. Jiang, U. E. Aharodnikau, K. Yunusov, Y. F. Sun, T. Q. Liu, S. O. Solomevich, *Macromol. Rapid Comm.* **2022**, *43*, 2200037.

[31] Z. Y. Zeng, G. H. Jiang, T. Q. Liu, G. Song, Y. F. Sun, X. Y. Zhang, *Bio-Des. Manuf.* **2021**, *4*, 902.

[32] G. Song, Y. F. Sun, T. Q. Liu, X. Y. Zhang, Z. Y. Zeng, R. F. Wang, P. F. Li, C. H. Li, G. H. Jiang, *Chem. Eng. J.* **2021**, *426*, 130790.

[33] Y. Q. Zhang, J. C. Yu, A. R. Kahkoska, J. Q. Wang, J. B. Buse, Z. Gu, *Adv. Drug Deliver. Rev.* **2018**, *139*, 51.

[34] X. Jin, D. D. Zhu, B. Z. Chen, M. Ashfaq, X. D. Guo, *Adv. Drug Deliver. Rev.* **2018**, *127*, 119.

[35] Y. Yin, W. Su, J. Zhang, W. P. Huang, X. Y. Li, H. X. Ma, M. X. Tan, H. H. Song, G. L. Cao, S. J. Yu, D. Yu, J. H. Jeong, X. Zhao, H. Li, G. J. Nie, H. Wang, *ACS Nano.* **2021**, *15*, 14347.

[36] K. van der Maaden, W. Jiskoot, J. Bouwstra, *J. Control. Release.* **2012**, *161*, 645.

[37] P. C. DeMuth, J. J. Moon, H. Suh, P. T. Hammond, D. J. Irvine, *ACS Nano.* **2012**, *6*, 8041.

[38] S. Kusama, K. Sato, Y. Matsui, N. Kimura, H. Abe, S. Yoshida, M. Nishizawa, *Nat. Commun.* **2021**, *12*, 658.

[39] Z. Y. Wang, J. Y. Luan, A. Seth, L. Liu, M. L. You, P. Gupta, P. Rathi, Y. X. Wang, S. S. Cao, Q. S. Jiang, X. Zhang, R. Gupta, Q. J. Zhou, J. J. Morrissey, E. L. Scheller, J. S. Rudra, S. Singamaneni, *Nat. Biomed. Eng.* **2021**, *5*, 64.

[40] X. X. Zhang, G. P. Chen, F. K. Bian, L. J. Cai, Y. J. Zhao, *Adv. Mater.* **2019**, *31*, 1902825.

[41] J. J. Chi, X. X. Zhang, C. W. Chen, C. M. Shao, Y. J. Zhao, Y. A. Wang, *Bioact. Mater.* **2020**, *5*, 253.

[42] X. X. Zhang, G. P. Chen, Y. X. Liu, L. Y. Sun, L. Y. Sun, Y. J. Zhao, *ACS Nano.* **2020**, *14*, 5901.

[43] S. -J. Yang, J. -O. Jeong, Y. -M. Lim, J. -S. Park, *Mater. Design.* **2021**, *201*, 109485.

[44] S. P. Sullivan, D. G. Koutsonanos, M. D. P. Martin, J. W. Lee, V. Zarnitsyn, S. -O. Choi, N. Murthy, R. W. Compans, I. Skountzou, M. R. Prausnitz, *Nat. Med.* **2010**, *16*, 915.

[45] M. Z. Xing, X. Wang, L. C. Zhao, Z. Q. Zhou, H. Liu, B. R. Wang, A. Cheng, S. H. Zhang, Y. H. Gao, *Int. Pharmaceut.* **2021**, *600*, 120406.

[46] H. X. Wang, W. S. Wang, C. P. Li, A. Xu, B. S. Qiu, F. F. Li, W. P. Ding, *Chem. Eng. J.* **2022**, *428*, 131913.

[47] Y. Hao, Y. W. Chen, X. L. He, F. Yang, R. X. Han, C. L. Yang, W. Li, Z. Y. Qian, *Bioact. Mater.* **2020**, *5*, 542.

[48] P. C. DeMuth, Y. Min, B. Huang, J. A. Kramer, A. D. Miller, D. H. Barouch, P. T. Hammond, D. J. Irvine, *Nat. Mater.* **2013**, *12*, 367.

[49] X. F. Li, Q. A. Xu, J. Wang, P. Zhang, Y. X. Wang, J. Ji, *J. Mater. Chem. B.* **2021**, *9*, 5528.

[50] N. H. Khan, M. Mir, L. Qian, M. Baloch, M. F. A. Khan, Asim-ur-Rehman, E. E. Ngowi, D. -D. Wu, X. -Y. Ji, *J. Adv. Res.* **2022**, *36*, 223.

[51] X. C. Wang, I. S. Mohammad, L. F. Fan, Z. M. Zhao, M. Nurunnabi, M. A. Sallam, J. Wu, Z. J. Chen, L. F. Yin, W. He, *Acta Pharm. Sin. B.* **2021**, *11*, 2585.

[52] N. N. Aung, T. Ngawhirunpat, T. Rojanarata, P. Patrojanasophon, P. Opanasopit, B. Pamornpathomkul, *AAPS PharmSciTech.* **2020**, *21*, 25.

[53] R. Obaidat, F. BaniAmer, S. M. Assaf, A. Yassin, *AAPS PharmSciTech.* **2021**, *22*, 253.

[54] W. C. Sun, Z. Araci, M. Inayathullah, S. Manickam, X. X. Zhang, M. A. Bruce, M. P. Marinkovich, A. T. Lane, C. Milla, J. Rajadas, M. J. Butte, *Acta Biomater.* **2013**, *9*, 7767.

[55] S. -J. Yang, J. -O. Jeongm, Y. -M. Lim, J. -S. Park, *Mater. Design.* **2021**, *201*, 109485.

[56] J. Lu, N. Dalbeth, H. Y. Yin, C. G. Li, T. R. Merriman, W. -H. Wei, **2019**, *15*, 413.

[57] D. -C. Tarng, H. -Y. Lin, M. -L. Shyong, J. -S. Wang, W. -C. Yang, T. -P. Huang, *Am. J. Nephrol.* **1995**, *15*, 31.

[58] F. Perez-Ruiz, J. S. Sundy, J. N. Miner, M. Cravets, C. Storgard, *Ann. Rheum. Dis.* **2016**, *75*, 1074.

[59] D. Pitocco, E. Di Stasio, F. Romitelli, F. Zaccardi, B. Tavazzi, A. Manto, S. Caputo, T. Musella, C. Zuppi, S. A. Santini, G. Ghirlanda, *Diabetes-Metab. Res.* **2008**, *24*, 318.

[60] R. Dhouibi, H. Affes, M. Ben Salem, D. Moalla, R. Marekchi, S. Charfi, S. Hammami, Z. Sahnoun, K. Jamoussi, K. M. Zeghal, K. Ksouda, *Life Sci.* **2021**, *268*, 118998.

[61] M. X. Pang, Y. Y. Fang, S. H. Chen, X. X. Zhu, C. W. Shan, J. Su, J. J. Yu, B. Li, Y. Yang, B. Chen, K. L. Liang, H. M. Hu, G. Y. Lv, *Med. Sci. Monitor.* **2017**, *23*, 1129.

[62] Y. Zhang, L. L. Deng, C. M. Wu, L. J. Zheng, G. Zhong, *J. Funct. Foods.* **2018**, *48*, 566.

[63] Y. Lee, P. Werlinger, J. -W. Suh, J. H. Cheng, *Microorganisms.* **2022**, *10*, 851.